Available online at www.sciencedirect.com
ScienceDirect
Polymer 49 (2008) 1716–1724
polymer
www.elsevier.com/locate/polymer

Surface adsorption of comb polymers by Monte Carlo simulations

Stefano Elli [a], Giuseppina Raffaini [a], Fabio Ganazzoli [a,*], Edward G. Timoshenko [b,1], Yuri A. Kuznetsov [b]

[a] *Dipartimento di Chimica, Materiali e Ingegneria Chimica ''G. Natta'', Politecnico di Milano, via L. Mancinelli 7, 20131 Milano, Italy*
[b] *Laboratory of Biomolecular Conformations, Centre for Synthesis and Chemical Biology, Conway Institute of Biomolecular and Biomedical Research, School of Chemistry and Chemical Biology, University College Dublin, Belfield, Dublin 4, Ireland*

Received 28 September 2007; received in revised form 23 January 2008; accepted 23 January 2008
Available online 1 February 2008

Abstract

This paper reports off-lattice Monte Carlo simulations of highly-branched comb homopolymers weakly adsorbed on a flat, featureless surface showing only covolume and dispersion interactions with the adsorbate. A minimal coarse-grained model, described by hard spheres connected by harmonic springs, was employed. The interaction energy of the adsorbed combs and linear chains is first discussed as a function of the molecular mass and of the number of beads in contact with the surface. The molecular size is then investigated as a function of backbone length and branching density at a fixed arm size. The apparent swelling exponents of the adsorbed combs are larger than those of the corresponding linear chains, and much larger than that of the free molecules. This result indicates a surface-induced stiffening of the comb backbone, further studied through the persistence length l_{pers}. It is found that l_{pers} increases upon adsorption over the free-molecule value, more so the larger is the branching density. Finally, the thickness of the adsorbed layer, the surface-induced molecular anisotropy and the molecular aspect ratio are investigated as a function of branching density and molecular mass.

Keywords: Surface adsorption; Comb polymers; Monte Carlo simulations

1. Introduction

Regular comb polymers, in particular those with a large density of branching, arose a great interest in the last years due to their conformational properties, in particular the backbone stiffness and the possibility to control it by changing the density of branching and the length of the side chains [1–6]. This feature of an enhanced rigidity due to covolume repulsions among the side chains was recently referred to as 'topological' stiffness [7], which may add to the 'intrinsic' stiffness of the backbone due to the local chemical structure. Highly-branched combs, sometimes called ''bottle-brushes'' were synthesized and experimentally characterized, and their stiffness was exploited, for instance, for obtaining new nanostructures or for templates in producing metallic nanowires [3,8,9].

Due to the large backbone rigidity, these molecules are quite anisotropic and may show lyotropic main-chain liquid-crystalline behaviour in semidilute or concentrated solutions [10]. Moreover, highly-branched combs display a pronounced two-dimensional (2D) ordering on a surface [11] that can be characterized and visualized by atomic force microscopy after depositing the molecules on a flat surface (typically mica or graphite) [9,11–13]. A large interest is also devoted to polymer adsorption as a way to control the properties of a surface (its hardness, wettability, and chemical stability, for instance). For example, specifically tailored hydrophilic polymers such as poly(vinyl alcohol) or poly(ethylene glycol) are used as surface coatings to prevent unwanted protein adsorption on charged or hydrophobic surfaces [14]. Linear or branched polymers are being used for this purpose, and a recent work dealt with the adsorption of comb copolymers with an adsorbing backbone

* Corresponding author. Tel.: +39 0223993024; fax: +39 0223993080.
E-mail addresses: fabio.ganazzoli@polimi.it (F. Ganazzoli), edward.timoshenko@ucd.ie (E.G. Timoshenko).
[1] Tel: +353 1 716 2821; fax: +353 1 716 2127.

0032-3861/$ - see front matter © 2008 Elsevier Ltd. All rights reserved.
doi:10.1016/j.polymer.2008.01.058

and repulsive side chains [15] as coating materials for bioseparations, for instance in capillary electrophoresis. However, a qualitatively similar effect can be expected in comb homopolymers, because the free ends of the side chains undergo a weaker adsorption than the backbone for entropic reasons.

Since surface adsorption constrains the comb conformation, further enhancing the apparent molecular stiffness, theoretical and simulation studies often considered the limiting case of strictly 2D combs [16,17], even though the surface adsorption of combs in 3D (three dimensional) was also modelled with a lattice Monte Carlo (MC) method [18]. Off-lattice simulations studied the related, but a distinct, problem of the confinement of combs between impenetrable, but otherwise non-interacting parallel plates [19]. Analytical approaches to study the surface adsorption of combs considered 2D molecules in the regime of strong adsorption, and the conformational properties were obtained by free-energy minimization [17]. In this way, the observed backbone curvature in a dense monolayer of highly-branched combs could be explained through the elasticity of the side chains.

However, in general the surface adsorption of macromolecules cannot be strictly 2D due to the entropic freedom of the end beads. Moreover, even with very long side chains, where end effects are negligible, and in the limit of strong adsorption, a fully 2D structure may not be achieved in practice for kinetic reasons, and self-overlap of the single molecule would easily be obtained. For these reasons, we carried out an off-lattice MC simulation in 3D of the adsorption of comb homopolymers on a smooth, continuous surface aimed to characterize *inter alia* the backbone stiffness. In the next section, we report the simulation methodology, which represents an extension of the method previously adopted to study isolated combs [6]. We then turn to the main results, by first discussing the interaction energy of the adsorbed combs, and then their molecular size through the mean-square end-to-end distance and radius of gyration of the backbone. Finally, we consider the backbone persistence length, the thickness of the adsorbed molecules and the molecular aspect ratio.

2. Simulation methodology

2.1. The system Hamiltonian

We adopt a bead-and-spring model with a hard-sphere interaction potential to describe the excluded-volume interactions, assuming an athermal solvent. This coarse-grained model can be viewed as the minimal model that still captures the main physical features of the system at a large scale. For a free molecule in 3D space, the system Hamiltonian is given by [6,20]:

$$H = \frac{k_B T}{2\ell^2}\sum_{i\sim j} r_{ij}^2 + \frac{1}{2}\sum_{i\neq j} V(r_{ij}) \tag{1}$$

where $r_{ij} = |\mathbf{X}_i - \mathbf{X}_j|$ is the instantaneous inter-bead distance, $\mathbf{X}_i$ and $\mathbf{X}_j$ being the vector position of the i-th and j-th beads, respectively. In Eq. (1), the terms within the first sum account for the harmonic springs between the connected beads, indicated by $i \sim j$, and those within the second sum for the pairwise interaction potential. Adopting a hard-sphere potential, $V(r)$ is given by:

$$V(r) = \begin{cases} +\infty & \text{if } r < d \\ 0 & \text{if } r > d \end{cases} \tag{2}$$

where d is the sphere diameter. With the definition of the spring constant in Eq. (1), the mean-square distance between connected beads in a random walk is $\langle r_{i,i+1}^2 \rangle = 3\ell^2$. As previously done [20], in the following we use throughout the reduced units $k_B T = 1$ and $\ell = 1$, and take $d = \ell$ as a convenient choice.

We also assume that the adsorption substrate occupies the half-space $-\infty < z < 0$ and exposes a smooth, featureless surface that is infinite in the x, y directions, introducing a further term in the Hamiltonian. This term, expressed as $\sum_i w(D_i)$, depends only on the distance D_i of i-th bead from the surface, and therefore it is a one-body potential. We assume that each polymer bead interacts with a substrate 'molecule' through a Lennard–Jones 6-12 potential, $w_{6\text{-}12}^{\mathrm{LJ}}(r)$:

$$w_{6\text{-}12}^{\mathrm{LJ}}(r) = \varepsilon\left[\left(\frac{\sigma}{r}\right)^{12} - \left(\frac{\sigma}{r}\right)^{6}\right] \tag{3}$$

This potential contains two terms of the form $w_n(r) = -C_n/r^n$ (with $C_n > 0$ for $n = 6$ and $C_n < 0$ for $n = 12$). Following Ref. [21, p. 155–157], upon integration over all the substrate molecules we get from each term:

$$w_n(D) = \frac{2\pi C_n \rho}{(n-2)(n-3)}\frac{1}{D^{n-3}} \tag{4}$$

where ρ is the substrate density of 'molecules'. Therefore, the full potential accounting for both the attractive and the repulsive part becomes a 3-9 potential:

$$w(D) \equiv w_{3\text{-}9}(D) \frac{\pi\rho}{3}\varepsilon\sigma^3\left[\frac{1}{15}\left(\frac{\sigma}{D}\right)^9 - \frac{1}{2}\left(\frac{\sigma}{D}\right)^3\right] \tag{5}$$

which has a minimum for $D = (2/5)^{1/6}\sigma$ and vanishes for $D = (2/15)^{1/6}\sigma$. In practice, it is more useful to consider a soft but eventually impenetrable surface through a lower cut-off, so that the bead-surface potential becomes:

$$w(D) = \begin{cases} \infty & D < (2/15)^{1/16}\sigma \\ \dfrac{\pi\rho}{3}\varepsilon\sigma^3\left[\dfrac{1}{15}\left(\dfrac{\sigma}{D}\right)^9 - \dfrac{1}{2}\left(\dfrac{\sigma}{D}\right)^3\right] & D \geq (2/15)^{1/16}\sigma \end{cases} \tag{6}$$

and the shortest allowed bead-surface distance is $D = (2/15)^{1/6}\sigma$. Therefore, a bead with a diameter equal to ℓ might partially enter the surface. For this reason we parameterized the potential so that the minimum of $w(D)$ is found at $D_{\min} = 1/2$, whence:

$$\sigma = D_{\min}/(2/5)^{1/6} = 0.5825 \tag{7}$$

For simplicity, we further selected $\rho = 3/\pi$, while the ε parameter was chosen in the weak adsorption limit for practical reasons, since the equilibration times in the Monte Carlo simulations (see also later) do strongly increase with increasing ε.

In practice, we selected $\varepsilon = 19.092$, so that the potential minimum is:

$$w(D_{\min}) = -2.0\, k_B T \tag{8}$$

2.2. The adsorption criterion for physisorption

In real systems, the non-bonded interactions between a physisorbed molecule and a surface may be due to hydrogen bonds, dipolar interactions or dispersion forces, or more generally to their combination. Therefore, at room temperature, physisorption should be regarded as a reversible, dynamic equilibrium between surface-adsorbed and free molecules. Ideally, one should model a huge system with a large number of molecules that may adsorb and desorb from the surface to evaluate the equilibrium constant. Practically, our simulations only consider single molecules unbound in the x, y directions (thanks to periodic boundary conditions), confined in the $z > 0$ half-space and interacting with the surface at $z = 0$. Therefore, the configurational properties of an adsorbed molecule must be calculated from an appropriate subset of the configurations encountered after equilibration in a very long MC simulation run for an ergodic system, or, more efficiently, in different replica of equivalent shorter simulations. This problem is increasingly important with short chains, since the configurational entropy favouring desorption becomes more important than the interaction energy. We thus adopted an energetic criterion to select the adsorbed configurations for calculating the average properties of interest. If two molecules interact through a short-range Lennard–Jones potential, we can safely assume that the interaction is negligible when the separation r in Eq. (3) is $\geq 4\sigma$, so that:

$$w^{\mathrm{LJ}}_{6\text{-}12}(r = 4\sigma)/w^{\mathrm{LJ}}_{6\text{-}12}(r = r_{\min}) = 4^{-5} \tag{9}$$

Adopting the same criterion for the limiting distance $D_{\lim}$ of a significant surface potential, we have:

$$w_{3\text{-}9}(D_{\lim})/w_{3\text{-}9}(D_{\min}) = 4^{-5} \tag{10}$$

and solving this equation with respect to $D_{\lim}$ by Eq. (5) we obtain $D_{\lim} \cong 10\sigma$, or $D_{\lim} \cong 6$ by Eq. (7). Hence, we assume that a molecule is in a (weakly) adsorbed configuration whenever at least one of its beads lies at a distance $D < 6$ from the surface.

2.3. The size and topology of the modelled combs, and the simulation strategy

We consider combs with N_b backbone beads and $n_b = N_b - 1$ springs, containing f arms, each with N_a beads. The arms are evenly distributed along the backbone, and the total number of beads is $N = N_b + fN_a$. The branching density is $m = (N_f + 1)^{-1}$, where N_f is the number of beads between adjacent branch points, which reduces to $m = f/N_b$ in the long-chain limit. Here, we study both linear chains with $m = 0$ and highly-branched combs with $m = 0.25$, 0.5 and 1 (neglecting the end beads). The two latter combs, also referred to as 'bottle-brushes' for their large density of branching, were already studied in free space with the same model [6]. Note that for $m = 0$ or for $N_a = 0$ we get a linear chain with the same length as the comb backbone. In this study, we considered linear chains and combs with up to $N = 350$ (for the combs with $m = 1$ we also considered the case $N = 590$ and $N_b = 100$), the combs having a backbone length up to $N_b = 100$ and $N_a = 5$ in all cases.

The simulations employ the MC method in continuous 3D space using the standard Metropolis algorithm as described in previous papers [6,20]. The procedure involves random local moves of a randomly selected bead with a minimum displacement of 0.1 (in ℓ units) adjusted to achieve an acceptance ratio very close to 0.5 to avoid non-ergodicity in the phase-space sampling. Due to the excluded-volume constraint and the presence of the surface, the number of rejected moves was somewhat larger than in the free state, but still the acceptance ratio was never lower than 0.49. As starting geometries, stretched conformations were generated in the $z = 2$ plane, and then equilibrated with the MC method monitoring the relaxation time through the changes in the instantaneous squared radius of gyration of the molecule S^2: one relaxation time was taken as equal to twice the time (or number of moves) required to achieve a constant S^2, apart from fluctuations, starting from the initial geometry. The data collection was then carried out saving the instantaneous geometries of a large number of almost independent configurations to calculate the statistical averages. These configurations were separated by a large number of sweeps ($\sim N^2$, a sweep corresponding to N attempted moves) corresponding to a single relaxation time, but in a few cases many configurations were still found to be correlated. This ergodicity problem is related to the surface constraint, and the procedure was repeated by generating up to 10 independent samples through independent relaxation of the initial geometry and then collecting the data at intervals equal to one half of the relaxation time for convenience, even though in principle minor correlations could still be found between consecutive samples.

2.4. The measured quantities

We first discuss the interaction energy E_{int} (in $k_B T$ units), defined as:

$$E_{\mathrm{int}} = E_{\mathrm{free}} - E_{\mathrm{ads}} \tag{11}$$

where E_{free} and E_{ads} are the average energies of the free and adsorbed molecules, respectively, since as introduced by us the bare surface has a nil constant energy. According to this definition, E_{int} is positive for an adsorbed molecule and corresponds to the energy required to desorb it to the free equilibrium state. In particular, we study the dependence of E_{int} on the average number of beads in contact with the surface, N_{surf}, and on the backbone beads N_b or the total number of beads N. In turn, N_{surf} is given by the average number of beads found in the first layer at a unit distance from the surface.

The average quantities characterizing the molecular size are the mean-square distances among the backbone beads, $\langle r^2_{ij} \rangle$,

and the mean-square end-to-end distance $\langle R_b^2 \rangle$ and radius of gyration $\langle S_b^2 \rangle$ of the backbone:

$$\langle S_b^2 \rangle = \frac{1}{2N_b^2} \sum_{i,j=1}^{N_b} \left\langle r_{ij}^2 \right\rangle \tag{12}$$

The chain stiffness is characterized through the backbone persistence length. Among the possible definitions, as done before [6] we adopt the projection of the backbone end-to-end vector $\mathbf{R}_b$ on the generic k-th spring [6,7,22]:

$$l_{pers}^{(k)} = \left\langle \frac{\mathbf{r}_{k,k+1}}{|\mathbf{r}_{k,k+1}|} \right\rangle \cdot \mathbf{R}_b \tag{13}$$

where $l_{pers}^{(k)}$ may depend on the spring location within the backbone.

The thickness of adsorbed molecules is described through the z-component of the radius of gyration orthogonal to the surface in the $z = 0$ plane, or more precisely through the average value of the zz-component of the radius of gyration tensor, $\langle S_{zz}^2 \rangle$:

$$\langle S_{zz}^2 \rangle = \left\langle \frac{1}{N} \sum_{i=1}^{N} (X_{z,i} - \overline{X}_z)^2 \right\rangle \tag{14}$$

where $\overline{X}_z$ is the z-component of the vector position of the molecular centre of mass:

$$\overline{X}_z = \frac{1}{N} \sum_{i=1}^{N} X_{z,i} \tag{15}$$

Finally, the molecular anisotropy is characterized by the ratio A between the average size perpendicular to the surface and the parallel ones, using the diagonal components of the radius of gyration tensor:

$$A = \frac{\langle S_{zz}^2 \rangle}{\frac{1}{2}\left(\langle S_{xx}^2 \rangle + \langle S_{yy}^2 \rangle \right)} \tag{16}$$

where x, y are the directions parallel to the surface. The A ratio measures the surface-induced anisotropy in the laboratory frame of reference, since the eigenvalues of the radius of gyration tensor are not used. For an average spherical shape Eq. (16) yields $A = 1$, while $A = 0$ would correspond to an infinitely thin disc, if $\langle S_{xx}^2 \rangle = \langle S_{yy}^2 \rangle$ remain finite.

3. Results and discussion

3.1. The interaction energy

The interaction energy E_{int} defined in Eq. (11) is first studied as a function of the number of beads in contact with the surface, N_{surf}. Since the surface interactions are described through additive dispersion forces only, E_{int} linearly increases with N_{surf}, basically with no dependence from topology. In fact, the data points (not shown for brevity) do follow a universal behaviour, and can be accurately fitted by straight lines through the origin with essentially the same slope. These slopes give the interaction energy per bead in contact with the surface, and are slightly smaller than the depth of the potential minimum in Eq. (8). In fact, their values are 1.708(5) for the linear chain, 1.691(10) for the comb with $m = 0.5$, and 1.670(14) for the comb with $m = 1$, the correlation coefficient being always $R > 0.9999$ (the figures in parentheses are the estimated standard errors on the last significant digits obtained by weighted regression). These values indicate a weak trend towards a smaller E_{int} with an increasing branching density m, but the differences are not statistically significant at the 3σ level. On the other hand, E_{int} linearly depends on the number of backbone beads N_b, strongly increasing with an increasing branching density m (data not shown), because more beads interact with the surface thanks to the molecular topology. It is of greater interest, however, to plot E_{int} as a function of the total number of beads N, as shown in Fig. 1. The figure shows that for a given N the linear chains have a larger E_{int} than combs, whose interaction weakens with increasing m. This result can be explained considering that for a fixed N a larger branching density, i.e., more side chains, implies more terminal beads that are not adsorbed for entropic reasons, whence the smaller interaction energy.

In conclusion, for a given backbone length combs show a stronger adsorption than linear chains, whereas the opposite is true for a given molecular mass due to the large number of free ends that are not fully adsorbed. This feature is relevant when hydrophilic polymers are used as coatings of hydrophobic surfaces to prevent the unwanted adsorption of proteins or of other biological macromolecules, for instance in analytical separation techniques [14,15].

3.2. The molecular size

The size of the adsorbed molecules is described through the backbone mean-square end-to-end distance, $\langle R_b^2 \rangle$, and radius

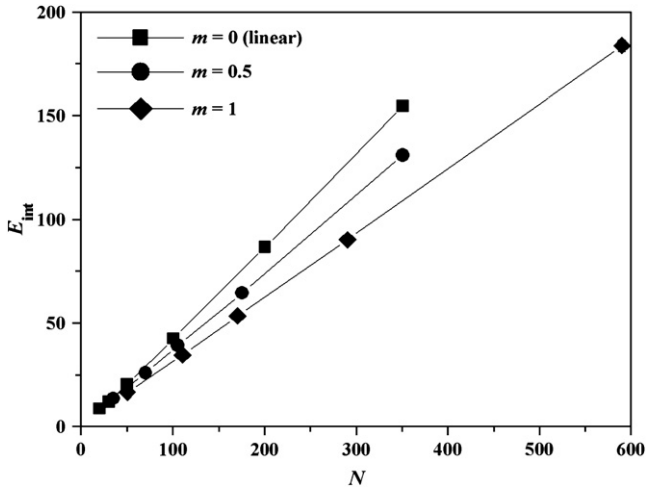

Fig. 1. The interaction energy E_{int} plotted as a function of the total number of beads N for linear chains (squares) and combs with branching densities $m = 0.5$ (circles) and 1 (diamonds). The backbone lengths are in the range $10 \leq N_b \leq 100$. The error bars on E_{int} are smaller than the symbol sizes.

of gyration, $\langle S_b^2 \rangle$, and are shown in Fig. 2 (empty and filled symbols, respectively) as a function of the number of the backbone springs n_b. As expected, combs have a larger size than the linear chains with the same n_b, with an increasingly stronger dependence on the branching density m and the backbone length n_b due to the increased excluded volume among the arms. In fact, for the longer chains, the data points can be fitted with the power law:

$$\langle X^2 \rangle = a_x n_b^{2\nu_x} \tag{17}$$

where X is either R_b or S_b, and ν_x is the corresponding swelling exponent (solid and dashed lines in Fig. 2). The weighted best-fit values of a_x and ν_x are reported in Table 1. The larger exponents for highly-branched combs compared to linear chains are already evident from the slopes of the fitting lines in the log–log plot.

Fig. 2 shows also that in the adsorbed chains the swelling exponents ν_x do change with the backbone length, both for $\langle R_b^2 \rangle$ and for $\langle S_b^2 \rangle$, and ν_R is larger than ν_S (see Table 1), even though the difference is not statistically significant at the 3σ level. All the exponents are significantly larger than the value we obtained for the mean-square end-to-end distance of a free linear chain, namely $\nu = 0.588(2)$ [6], equal in turn to the best current theoretical value of 0.5882(11) [23]. Still, for the linear chains, they are smaller than the theoretical value for self-avoiding walks in 2D, namely $\nu = 0.75$ exactly [24]. A similar trend was also found through off-lattice MC simulations for 2D linear chains by Freire et al. [25], who obtained critical exponents larger than ours, but still with $\nu_S < \nu_R < 0.75$, the differences being larger than the estimated standard errors. On the other hand, other off-lattice MC simulations obtained a different result, namely that athermal short linear chains with $N \leq 30$ already showed an exponent of 0.750(3) for the mean-square end-to-end distance in 2D, unlike what found in 3D where an apparent exponent of 0.638(3) was obtained [19]. Crossover exponents and finite size effects could partly account for such differences, but the detailed explanation is not quite clear as yet, in our opinion.

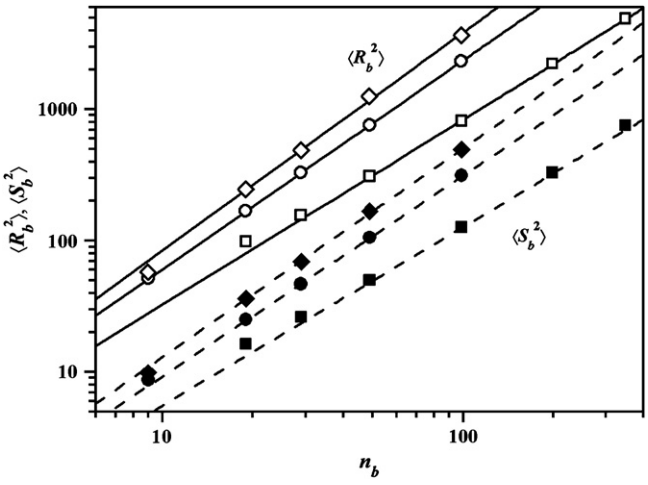

Fig. 2. The backbone mean-square end-to-end distance $\langle R_b^2 \rangle$ (empty symbols), and radius of gyration $\langle S_b^2 \rangle$ (filled symbols) plotted as a function of the number of the backbone springs n_b. The squares indicate linear chains, while the circles and the diamonds refer to combs with branching densities $m = 0.5$ and 1, respectively, with a side-chain length of $N_a = 5$ beads. In all cases, the error bars are smaller than the symbol size. The combs with $m = 0.25$ are not reported for clarity. The solid and dashed lines are the power-law fitting curves obtained by weighted regression according to Eq. (17), obtained by ignoring the shorter chains. The best-fit parameters are reported in Table 1.

Table 1
The fitting parameters of Eq. (17) obtained by weighted regressions for linear chains ($m = 0$) and combs with $N_a = 5$ beads per arm and a varying degree of branching m

m	$\langle R_b^2 \rangle$[a]		$\langle S_b^2 \rangle$[b]		$\langle r_{ij}^2 \rangle$[c]	
	a_R	ν_R	a_S	ν_S	a_{ij}	ν_{ij}
0	1.25(13)	0.705(11)	0.24(1)	0.682(6)	2.52(4)	0.648(2)
0.25	1.04(10)	0.796(12)	0.21(1)	0.753(7)	2.08(9)	0.748(6)
0.5	1.54(8)	0.796(8)	0.27(1)	0.767(6)	2.55(5)	0.765(3)
1	1.83(12)	0.831(10)	0.33(14)	0.795(6)	2.99(8)	0.812(4)

The standard errors on the last significant digit(s) are reported in parentheses.
[a] Mean-square end-to-end distance of the backbone.
[b] Mean-square radius of gyration of the backbone.
[c] Mean-square distance between beads i and j of the backbone. For all topologies, a constant backbone length of $N_b = 100$ beads was used.

The discrepancy between our ν_x values and the theoretical one in 2D can be rationalized by considering that our adsorption criterion is relatively loose, since chain configurations with only few adsorbed beads are included in the calculations. In fact, our interaction potential is weakly attractive, so that a significant fraction of monomers forms 'loops' instead of 'trains' (Fig. 3), with large deviations from a 2D system. Moreover, the convergence of the critical exponents ν_x to the asymptotic values appears to be quite slow in 2D, so that Table 1 only reports apparent critical exponents. We checked that upon strongly increasing the surface attraction by choosing a larger ε so that $w(D_{min}) = -10.0\, k_B T$ in Eq. (8), the apparent swelling exponents increase to $\nu_R = 0.735(7)$ and $\nu_S = 0.710(4)$, but the ergodicity problems (i.e., the kinetic trapping of the chain in an almost frozen adsorbed state) become serious even for linear chains. Therefore, we may expect that in strong attractive condition the exponent should converge to the theoretical value of 0.75 in 2D. The fact remains that the ν_R and ν_S exponents for finite combs are larger than for the corresponding linear chains, and increase with the branching density, even though in some cases the differences are within the statistical uncertainty.

Another estimate of the critical exponents is provided by mean-square distances among the backbone beads, $\langle r_{ij}^2 \rangle$, plotted as a function of the topological separation $|i - j|$ in Fig. 4 at a fixed backbone length ($N_b = 100$). Neglecting neighbouring beads, the data were fitted by the power-law equation (Eq. (17)), after replacing n_b with $|i - j|$ (solid lines in Fig. 4), and the resulting ν_{ij} and a_{ij} values are reported in Table 1. For the linear chain, ν_{ij} is smaller than ν_R and ν_S, whereas $\nu_{ij} = \nu_S$ in

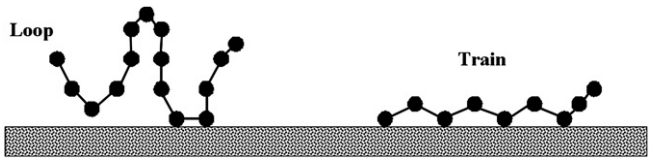

Fig. 3. Sketch of the loops and trains than can be formed by adsorbed chains.

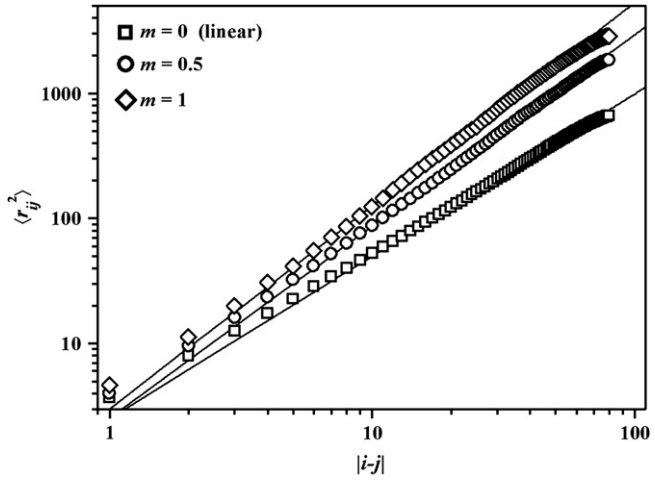

Fig. 4. The mean-square distances among the beads $\langle r_{ij}^2 \rangle$ plotted as a function of the topological separation $|i-j|$ for combs with $N_b = 100$ and a different density of branching. The squares indicate linear chains, while the circles and the diamonds refer to combs with branching densities $m = 0.5$ and 1, respectively, with a side-chain length of $N_a = 5$ beads. In all cases, the error bars are smaller than the symbol size. The combs with $m = 0.25$ are not reported for clarity. The solid lines are the power-law fitting curves according to Eq. (17), ignoring the end beads. The best-fit parameters are reported in Table 1.

combs with $m = 0.25$ and 0.5, both exponents being smaller than ν_R. In the highly-branched comb with $m = 1$ we find the inequality $\nu_S < \nu_{ij} < \nu_R$, although the differences are not statistically significant at the 3σ level. The exponents show that in all systems the mean-square end-to-end distance increases with n_b faster than the mean-square distances among the internal beads, hence also faster than the mean-square radius of gyration. Such observation suggests that the end-to-end distance will achieve its asymptotic values more quickly than the radius of gyration, as already found for free molecules [6]. Therefore, the exponents reported in Table 1 would slowly change with increasing n_b, the different values being due to the chain finiteness. For this reason, the ν_{ij} exponents are also plotted as a function of n_b^{-1} in Fig. 5. At least for linear chains, our extrapolated

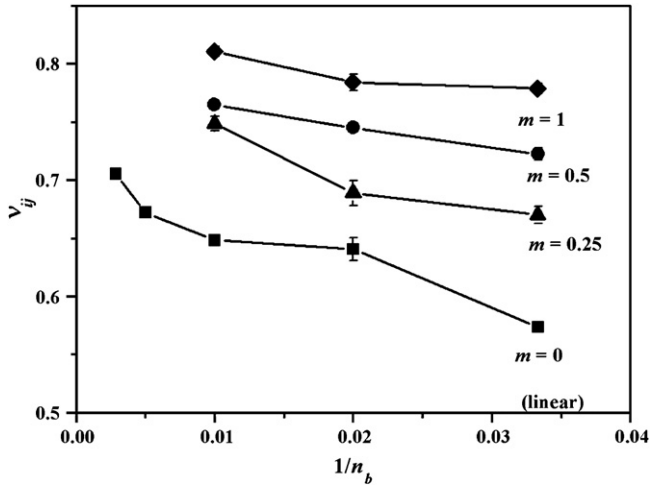

Fig. 5. The Flory exponent ν_{ij} plotted as a function of n_b^{-1} for linear chains (squares) and combs with a varying density of branches m and an arm length of $N_a = 5$ beads.

results are consistent with the theoretical value of 0.75. Compared to what we obtained for free chains, where the theoretical value is already achieved by backbone lengths with as few as 100 beads [6], an adsorbed chain attains the asymptotic behaviour at a very large molecular mass, possibly outside the experimental range. As for the combs, the plots in Fig. 5 indicate that no extrapolation may be confidently performed from finite molecules. In principle, we expect that infinitely long combs with a finite and constant side-chain length eventually achieve the theoretical value $\nu = 0.75$, independent of branching density. However, such asymptotic behaviour is not apparent in our simulations, and we suggest that the same problem is also experimentally met.

3.3. The stiffness of the adsorbed molecules and the backbone persistence length

The stiffness of the adsorbed molecules was studied through the backbone persistence length, defined in Eq. (13), in comparison with the analogous quantity for the free molecules [6,7]. This definition, particularly suited for finite chains, generalizes the original one due to Flory [22]. According to Eq. (13), the persistence length $l_{pers}^{(k)}$ is the average projection of the end-to-end vector $\mathbf{R}_b$ on the generic k-th backbone spring, and therefore it depends on k. The persistence lengths of adsorbed chains are shown in Fig. 6 as a function of k in comparison with those of the free molecules. In all cases, $l_{pers}^{(k)}$ has a maximum for intermediate k, and it displays small values near the chain ends ($k \approx 1$ and $k \approx n_b$). This is due to the greater configurational freedom of the end beads, often not adsorbed for entropic reasons, so that the persistence length of the end springs is not affected by branching or adsorption. Apart from these end effects, upon adsorption the backbone stiffness increases with branching more strongly than in free molecules, and we do not find an extended plateau in the central part of the plots of $l_{pers}^{(k)}$ vs. k.

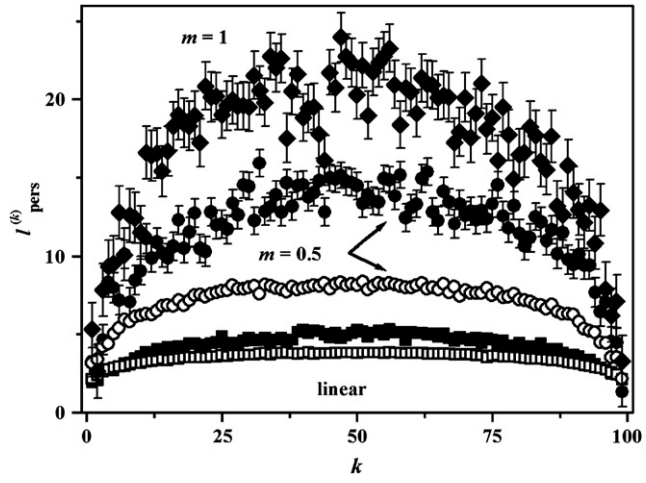

Fig. 6. The persistence length $l_{pers}^{(k)}$ plotted as a function of the spring location k within the chain backbone ($k = 1$ and $N_b - 1$ are the terminal springs) for the adsorbed chains (filled symbols) and the free chains (open symbols) for comparison. In all cases the backbone length was $N_b = 100$, and the arm length of the combs was $N_a = 5$. The data apply to linear chains (squares) and combs with $m = 0.5$ (circles) and 1 (diamonds). The data for the free comb with $m = 1$ are not reported for clarity.

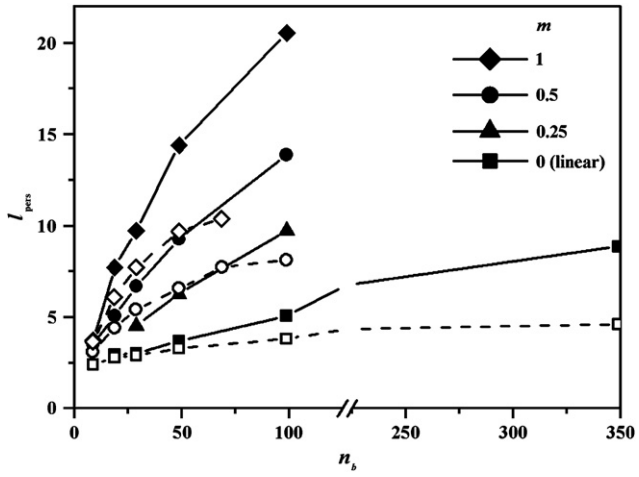

Fig. 7. The effective persistence length l_{pers} plotted as functions of the number of backbone springs n_b for linear chains ($m = 0$, squares) and combs with $N_a = 5$ beads per arm and different branching densities: $m = 0.25$ (triangles), 0.5 (circles), and 1 (diamonds). The filled symbols apply to the adsorbed molecules, and the empty symbols to the free ones. The solid lines are only guides for the eye.

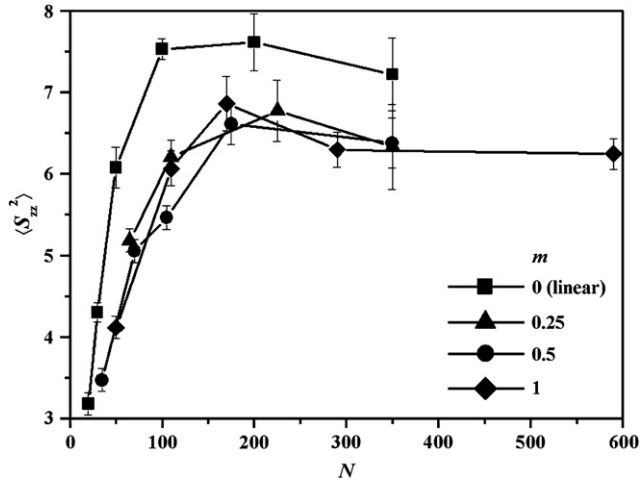

Fig. 9. The mean-square thickness of the adsorbed molecules defined by the component of the mean-square radius of gyration perpendicular to the surface, $\langle S_{zz}^2 \rangle$, plotted as a function of the total number of beads N for linear chains (squares) and combs with $N_a = 5$ beads per arm and different branching densities: $m = 0.25$ (triangles), 0.5 (circles), and 1 (diamonds). The solid lines are only guides for the eye.

In order to characterize the backbone stiffness through an effective persistence length l_{pers} not affected by end effects, we average the $l_{pers}^{(k)}$ values over the central plateau, as done in previous work. Here we follow the same procedure, although this plateau is quite restricted. The resulting values of l_{pers} strongly increase with the backbone length n_b for a fixed arm length $N_a = 5$, as shown in Fig. 7 (filled symbols), achieving values much larger than for the corresponding free molecules (empty symbols). Moreover, l_{pers} increases also with the branching density m at a fixed backbone length as displayed in Fig. 8, the adsorbed molecules showing again a larger stiffness than the free molecules. These results clearly demonstrate that the backbone stiffness of linear chains and combs does significantly increase upon surface adsorption even at weak adsorption strength. Such behaviour may explain the experimentally observed liquid-crystalline ordering of highly-branched molecules (the molecular 'bottle-brushes') on atomically flat surfaces [11,13] (see next paragraph).

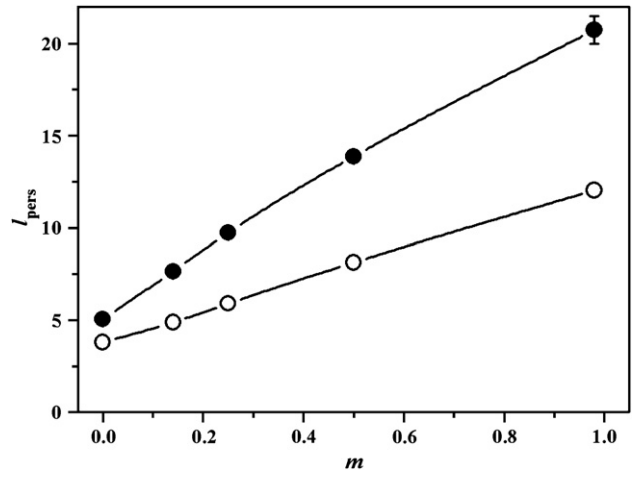

Fig. 8. The effective persistence length l_{pers} plotted as a function of the branching density m for linear chains ($m = 0$) and combs ($m > 0$, with a constant arm length $N_a = 5$) at a fixed backbone length $N_b = 100$ as free molecules (empty symbols) and adsorbed on a surface (filled symbols). The solid lines are only guides for the eye. When not shown, the error bars are smaller than the symbol size.

3.4. The molecular thickness at the interface and the aspect ratio of the adsorbed chains

The thickness of the adsorbed molecules is described through the zz-component of the radius of gyration tensor $\langle S_{zz}^2 \rangle$ of the whole molecule [Eq. (14)]. $\langle S_{zz}^2 \rangle$ is plotted in Fig. 9 as a function of the total number of beads N for linear chains and combs with a fixed arm length $N_a = 5$ and different branching densities m. In all cases, $\langle S_{zz}^2 \rangle$ increases with an increasing N to a maximum. After that, in combs, $\langle S_{zz}^2 \rangle$ levels off to a constant value independent of the branching density, suggesting that the same value is eventually achieved by linear chains. This behaviour should be attributed to an increasing number of beads that interact with the surface, which produce in turn a larger interaction energy (Fig. 1). Therefore, an increasing N enhances the surface spreading and adhesion, and the thickness of the adsorbed polymer layer becomes independent of the density of branching and eventually of topology.

On the other hand, at small N, the interaction energy with the surface is comparable to the entropy loss due to surface adsorption and the thickness of the adsorbed layer somewhat depends on topology. In fact, Fig. 9 shows that in this case the combs display a smaller thickness than linear chains for a given N due to the shorter backbone length. This feature can be explained by the larger probability of linear chains of forming loops instead of trains, the latter conformation being preferred by combs because of the larger bead density near the backbone due to branching. Such results do basically agree with those obtained through a self-consistent approach [26]. Therefore, based on this picture we obtain the general result

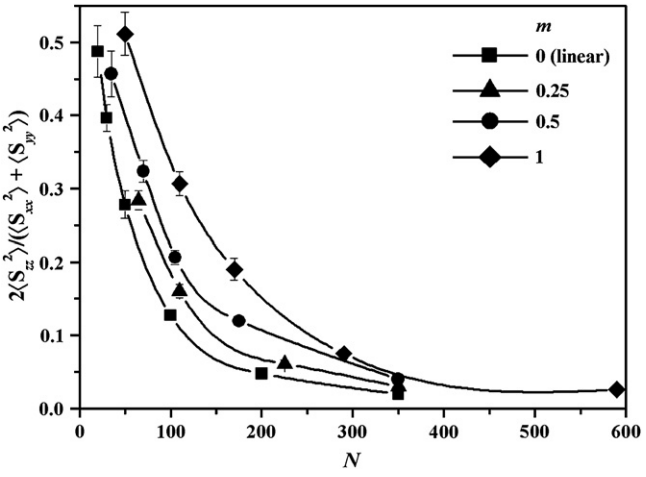

Fig. 10. The shape parameter A defined in Eq. (16) plotted as a function of the total number of beads N for linear chains (squares) and combs with $N_a = 5$ beads per arm and different branching densities: $m = 0.25$ (triangles), 0.5 (circles), and 1 (diamonds). The solid lines are splines through the data points used only for visual clarity.

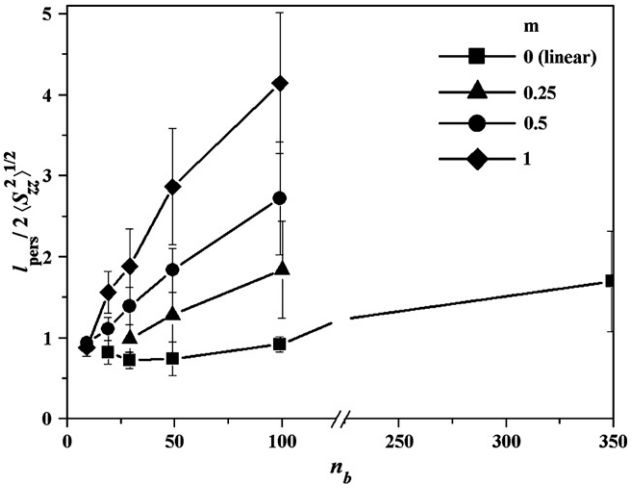

Fig. 11. The ratio $l_{pers}/2\langle S_{zz}^2\rangle^{1/2}$ plotted as a function of the number of backbone springs n_b for linear chains ($m = 0$, squares) and combs with $N_a = 5$ beads per arm and different branching densities: $m = 0.25$ (triangles), 0.5 (circles), and 1 (diamonds). The solid lines are only guides for the eye. This ratio slightly underestimates the molecular aspect ratio, as discussed in the text.

that highly-branched combs are better suited than linear chains to form thin layers on a surface in spite of the larger configurational freedom of the many free ends.

The anisotropy of the adsorbed molecules can be described through the A ratio defined in Eq. (16) and is shown as a function of N in Fig. 10. The plot shows that the shape distortion induced by the surface is quite severe for all topologies, and that A monotonically decreases with an increasing N in all cases. However, the molecular distortions from the spherical shape (in the laboratory frame of reference) monotonically decrease with an increasing branching density m, at a fixed N. Thus, the surface distortion is more evident for linear chains ($m = 0$), and becomes less pronounced for highly-branched combs as an effect of topology, in spite of their smaller thickness. In fact, the larger local density of monomers due to branching induces a larger local stiffness in 3D. However, a higher branching implies a shorter backbone length at a fixed N, and therefore the *relative* size enhancement parallel to the surface upon adsorption and the overall molecular deformation is somewhat smaller than for the linear chain. On the other hand, in weakly branched combs the opposite behaviour may be found, since a light branching may enhance the surface distortion because of the smaller stiffness, and the larger number of beads close to the backbone compared to linear chains.

Finally, Fig. 11 shows the ratio $l_{pers}/2\langle S_{zz}^2\rangle^{1/2}$ as a function of the number of backbone springs n_b. This ratio yields a reasonable estimate of the molecular aspect ratio, assuming that the molecular diameter of the adsorbed molecules is approximately given by twice the component of the radius of gyration perpendicular to the surface. Actually, since the molecules are not fully adsorbed, as previously discussed, $2\langle S_{zz}^2\rangle^{1/2}$ provides an upper bound for the true molecular diameter, so that in turn the calculated ratio somewhat underestimates the true molecular aspect ratio. In any case, Fig. 11 shows that the molecular aspect ratio of the adsorbed molecules strongly increases with the backbone length, more so the larger is the branching density, due to the analogous increase in l_{pers} (Fig. 7). Moreover, the values are also much larger than for the corresponding free molecules in 3D, where the aspect ratio was found to barely exceed unity.

The rapidly increasing behaviour of the molecular aspect ratio may explain the observation that highly-branched combs with very long backbones do form ordered liquid-crystalline domains on atomically flat surfaces [9,11–13]. In fact, theory predicts a lyotropic behaviour of semiflexible chains when the aspect ratio exceeds a value of 10 [27,28], consistent with the extrapolation to longer backbones of $l_{pers}/2\langle S_{zz}^2\rangle^{1/2}$ (which somewhat underestimates it).

4. Concluding remarks

In this paper, we study the adsorption of highly-branched combs on a flat and featureless surface in 3D by using off-lattice Monte Carlo simulations with a minimal coarse-grained model. The results are first discussed through the interaction energy with the surface and the molecular size with its (apparent) critical exponents. The data suggest that upon surface adsorption the asymptotic 2D behaviour is achieved more slowly than for the free molecules, in particular with combs. Such behaviour is related to the 'topological' stiffness due to the covolume repulsions among the side chains of the combs [6,7] that is significantly enhanced by surface adsorption. Accordingly, we also studied the persistence length of the backbone and its dependence on the branching density of the adsorbed molecules. The thickness and anisotropy of the adsorbed combs is also considered. It turns out that many terminal beads of the side chains in highly-branched combs are not adsorbed for entropic reason, thus decreasing somewhat the interaction energy with the surface compared to linear chains with the same molecular mass. However, we find the general result that highly-branched combs are better suited than linear chains to form thin adsorbed layers on a surface, since the presence of

the non-adsorbed free ends does not enhance the thickness of the adsorbed combs because it involves only a few beads. Moreover, we also show that the molecular aspect ratio strongly increases upon adsorption, becoming increasingly larger with an increasing branching density. Such result leads to predict the possibility of a 2D molecular ordering, in agreement with the experimentally observed pattern.

As final comments, we note that in the present paper we only considered relatively short side chains grafted to a much longer backbone. The opposite case of increasingly long side chains at a fixed backbone length would eventually correspond to a star polymer, thus loosing the topological specificity studied in the present paper. Also, we only considered the case of a weak adsorption. Increasingly long chains eventually show a strong-adsorption behaviour because of the additivity of the dispersive interactions. The strong bead-surface adsorption limit was briefly explored for linear chains, but it was not systematically explored for technical reasons. In fact, even with linear chains such situation leads to severe ergodicity problems with the present methodology that could possibly be overcome by different simulation strategies like the parallel tempering Monte Carlo method (see Ref. [29] for a recent review). On the other hand, we point out that this limit may also correspond experimentally to a non-ergodic system, with the adsorbed chains kinetically trapped in a glass-like state.

References

[1] Birshtein TM, Borisov OV, Zhulina YB, Khokhlov AR, Yurasova TA. Polym Sci USSR 1987;29:1293.
[2] Fredrickson GH. Macromolecules 1993;26:2825.
[3] Wintermantel M, Gerle M, Fischer K, Schmidt M, Wataoka I, Urakawa H, et al. Macromolecules 1996;29:978.
[4] Fischer K, Schmidt M. Macromol Rapid Commun 2001;22:787.
[5] Saariaho M, Subbotin A, Szleifer I, Ikkala O, ten Brinke G. Macromolecules 1999;32:4439;
Saariaho M, Ikkala O, ten Brinke G. J Chem Phys 1999;110:1180;
Saariaho M, Subbotin A, Ikkala O, ten Brinke G. Macromol Rapid Commun 2000;21:110.
[6] Elli S, Ganazzoli F, Timoshenko EG, Kuznetsov YuA, Connolly R. J Chem Phys 2004;120:6257.
[7] Connolly R, Bellesia G, Timoshenko EG, Kuznetsov YuA, Elli S, Ganazzoli F. Macromolecules 2005;38:5288.
[8] Tsukahara Y, Mizuno K, Segawa A, Yamashita Y. Macromolecules 1989;22:1546;
Tsukahara Y, Tsutsumi K, Yamashita Y, Shimada S. Macromolecules 1990;23:5201.
[9] Djalali R, Li S-Y, Schmidt M. Macromolecules 2002;35:4282.
[10] Wintermantel M, Fischer K, Gerle M, Ries R, Schmidt M, Kajiwara K, et al. Angew Chem Int Ed Engl 1995;34:1472.
[11] Dziezok P, Sheiko SS, Fischer K, Schmidt M, Möller M. Angew Chem Int Ed Engl 1997;36:2812.
[12] Gunari N, Schmidt M, Janshoff A. Macromolecules 2006;39:2219.
[13] Djalali R, Hugenberg N, Fischer K, Schmidt M. Macromol Rapid Commun 1999;20:444.
[14] Barrett DA, Hartshorne MS, Hussain MA, Shaw PN, Davies MC. Anal Chem 2001;73:5232.
[15] Sartori A, Johner A, Viovy J-L, Joanny J-F. Macromolecules 2005;38:3432.
[16] de Jong J, Subbotin A, ten Brinke G. Macromolecules 2005;38:6718.
[17] Potemkin II , Khokhlov AR, Prokhorova S, Sheiko SS, Möller M, Beers KL, et al. Macromolecules 2004;37:3918.
[18] Balazs AC, Siemasko CP. J Chem Phys 1991;95:3798.
[19] Saariaho M, Ikkala O, ten Brinke G. J Chem Phys 1999;110:1180.
[20] Ganazzoli F, Kuznetsov YuA, Timoshenko EG. Macromol Theory Simul 2001;10:325.
[21] Israelachvili J. Intermolecular and surface forces. London: Academic Press; 1992.
[22] Flory PJ. Statistical mechanics of chain molecules. New York: Wiley Interscience; 1969.
[23] Guida R, Zinn-Justin J. J Phys A 1998;31:8103.
[24] de Gennes P-G. Scaling concepts in polymer physics. Ithaca, NY: Cornell University Press; 1979.
[25] Torres AM, Rubio AM, Freire JJ, Bishop M, Clarke JHR. Macromolecules 1994;27:3483.
[26] van der Linden CC, Leermakers FAM, Fleer GJ. Macromolecules 1996;29:1000.
[27] Onsager L. Ann NY Acad Sci 1949;51:627.
[28] Khokhlov A, Semenov AN. Physica A 1981;108:546.
[29] Earl DJ, Deem MW. Phys Chem Chem Phys 2005;7:3910.